ADVANCES IN ATMOSPHERIC SCIENCES, VOL. 31, JULY 2014, 743–754

Model Simulations of Mesoscale Eddies and Deep Convection in the Labrador Sea

Jieshun ZHU[1], Entcho DEMIROV*[2], Ying ZHANG[3], and Ania POLOMSKA-HARLICK[2]

[1]*Center for Ocean–Land–Atmosphere Studies, George Mason University, Fairfax, Virginia, USA*
[2]*Department of Physics and Physical Oceanography, Memorial University of Newfoundland, St. John's, Newfoundland, Canada*
[3]*Department of Atmospheric and Oceanic Science, University of Maryland, College Park, Maryland, USA*

(Received 20 May 2013; revised 19 October 2013; accepted 6 December 2013)

ABSTRACT

Deep convection in the Labrador Sea is confined within a small region in the southwest part of the basin. The strength of deep convection in this region is related to the local atmospheric and ocean characteristics, which favor processes of deep convection preconditioning and intense air-sea exchange during the winter season. In this study, we explored the effect of eddy-induced flux transport on the stratification of the Labrador Sea and the properties of deep convection. Simulations from an eddy-resolving ocean model are presented for the Labrador Sea. The general circulation was well simulated by the model, including the seasonal cycle of the deep Labrador Current. The simulated distribution of the surface eddy kinetic energy was also close to that derived from Topex-Poseidon satellite altimeter data, but with smaller magnitude. The energy transfer diagnostics indicated that Irminger rings are generated by both baroclinic and barotropic processes; however, when they propagate into the interior basin, the barotropic process also disperses them by converting the eddy energy to the mean flow. In contrast to eddy-permitting simulations, deep convection in the Labrador Sea was better represented in the eddy-resolving model regarding their lateral position. Further analysis indicated that the improvement might be due to the lateral eddy flux associated with the resolved Irminger rings in the eddy-resolving model, which contributes to a realistic position of the isopycnal dome in the Labrador Sea and correspondingly a realistic site of deep convection.

Key words: mesoscale eddies, deep convection, labrador Sea, model simulation

Citation: Zhu, J. S., E. Demirov, Y. Zhang, and A. Polomska-Harlick, 2014: Model simulations of mesoscale eddies and deep convection in the Labrador Sea. *Adv. Atmos. Sci.*, **31**(4), 743–754, doi: 10.1007/s00376-013-3107-y.

1. Introduction

The Labrador Sea (Fig. 1) is a region with complex physical systems, and plays an important role in global climate dynamics due to its contribution to the Meridional Overturning Circulation (MOC). The general cyclonic circulation and strong oceanic winter heat loss make the occurrence of open ocean deep convection easy in the Labrador Sea, which results in the formation of Labrador Sea Water (LSW) (Marshall and Schott, 1999). Together with the Greenland–Scotland Overflow water originating from the mid-depths in the Nordic Seas, LSW contributes to the North Atlantic Deep Water (NADW), which acts as the lower limb of the global MOC (Gao and Yu, 2008).

Hydrographic data show that the deep convection in the Labrador Sea is confined within a small region in the southwest part of the basin (Lavender et al., 2000; Pickart et al., 2002; also see Fig. 1), where in certain years it can reach a depth of about 2000 m. Previous studies demonstrated that ocean circulation models (OGCMs) have limitations in representing deep convection in the Labrador Sea. Coarser-resolution models (Willebrand et al., 2001) and even some high-resolution simulations (Tréguier et al., 2005) often show excessive convection; that is, the mixed layer depth may almost reach the ocean bottom. Its lateral position is usually misrepresented by the non-eddy-resolving models (Zhu et al., 2010; Zhu and Demirov, 2011; Cook et al., 2014; also see section 5). The factors contributing to the OGCM biases of simulating deep convection are complex, and might include the uncertainties from the subscale parameterizations, surface forcing and unresolved physical processes. In this paper, we explore the impact of eddy-induced horizontal transport on the circulation and deep convection.

In the Labrador Sea, there are abundant mesoscale activities. According to Lilly et al. (2003), there are generally three types of eddies in the Labrador Sea: Irminger rings, convective eddies, and boundary current eddies. Among them, Irminger rings are the most energetic, which generates a maximum near coastal western Greenland on the eddy kinetic energy map (Lilly et al., 2003). In terms of the generation mechanisms, studies have shown that boundary current and

* Corresponding author: Entcho DEMIROV
Email: entcho@mun.ca

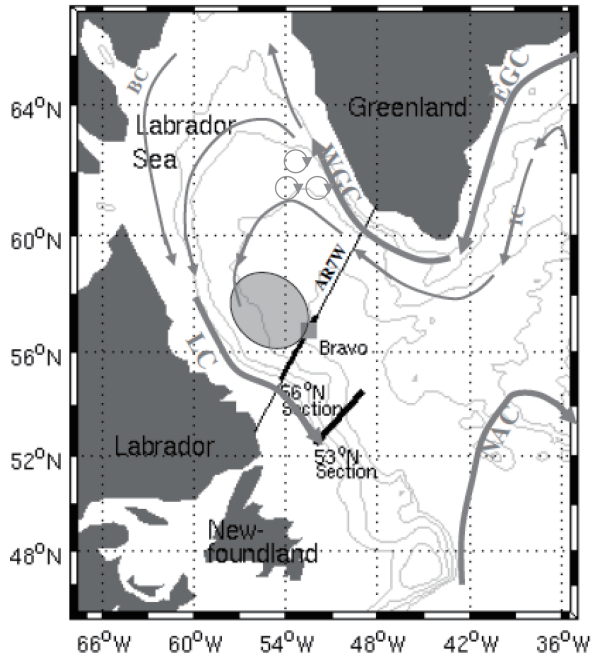

Fig. 1. Map of the Labrador Sea and its surroundings. The isobaths, shown by light contours, are 700, 2000, 3000 and 3500 m. Surface and near-surface current systems are depicted schematically by arrows (NAC: North Atlantic Current; EGC: East Greenland Current; WGC: West Greenland Current; LC: Labrador Current; IC: Irminger Current; BC: Baffin Island Current). The location of the deep convection site (shaded ellipse) is shown after Lavender et al. (2000) and Pickart et al. (2002). The two sections (namely, the 53°N and 56°N sections, indicated by black lines) perpendicular to the shelf break in the Labrador Sea are where the deep Labrador Currents were monitored repeatedly over the last decade (Dengler et al., 2006). Also marked are the locations of the former ocean weather station Bravo (square) and the WOCE AR7W hydrographic section (black line between Hamilton Bank, Labrador and Cape Desolation on the west coast of Greenland).

convective eddies are generated predominantly by the process of baroclinic instability of the cyclonic sub-polar gyre and the rim current around the mixed patched of deep convection waters (Eden and Böning, 2002). A considerable amount of studies have also been carried out regarding Irminger rings (Eden and Böning, 2002; Bracco and Pedlosky, 2003; Lilly et al., 2003; Katsman et al., 2004; Straneo, 2006; Hátún et al., 2007; Bracco et al., 2008; Chanut et al., 2008; Rykova et al., 2009). It has been identified that local bathymetry is important for their formation. However, the mechanism for the topography-triggered instability is still unclear. Particularly, depending on the study (Eden and Böning, 2002; Bracco and Pedlosky, 2003; Katsman et al., 2004; Bracco et al., 2008), their generation has been attributed to barotropic, baroclinic or mixed processes. Thus, further diagnostics are required to clarify this issue.

In this paper, we present results from an eddy-resolving model for the Labrador Sea. Our analysis focuses on the simulated mesoscale eddies and deep convection. To examine the intrinsic mechanism of Irminger rings, the baroclinic and barotropic mean-eddy flow energy transfer rates were calculated following the previous works of Wright (1981), Eden and Böning (2002) and Demirov and Pinardi (2007). Further, the impact of the mesoscale eddies on the positioning of deep convection in the Labrador Sea is also assessed by comparing the high-resolution run with one of our previous eddy-permitting simulations (Zhu et al., 2010). The paper is organized as follows. In section 2 the model setup and the datasets used are described. Section 3 briefly examines the general circulation in the Labrador Sea with a focus on the Deep Labrador Current. The simulated mesoscale eddies and deep convection in the Labrador Sea are analyzed in sections 4 and 5, respectively. The results presented in sections 3 and 4 are based on an eddy-resolving simulation, while in section 5 results from an eddy-permitting simulation are also examined to explore the effect of mesoscale eddies on the positioning of deep convection in the Labrador Sea. Section 6 presents a discussion and conclusions.

2. Model configurations and datasets

The numerical model used in the study was the NEMO (Nucleus for European Models of the Ocean; Madec, 2008) modeling system. It is a primitive equation, free surface ocean circulation code OPA9 (Ocean PArallelise version 9; Madec, 2008) coupled with the multi-layered sea-ice code LIM2 (Fichefet and Maqueda, 1997).

2.1. *A two-way nesting eddy-resolving system*

The simulations of the Labrador Sea were produced by an embedded system, in which a high-resolution (1/12)° Labrador Sea model (LAB12) was two-way nested within an eddy-permitting (1/4)° North Atlantic Model (NA025). The nesting algorithm was based on the AGRIF package (Adaptive Grid Refinement In FORTRAN; Blayo and Debreu, 1999; Debreu et al., 2005). The model parameters are summarized in Table 1.

The NA025 model (Zhu et al., 2010) covers the North Atlantic from 7°N to 67°N, with a Mercator isotropic grid

Table 1. Model parameters of the embedded system.

Name of model	Horizontal resolution	Horizontal dimensions	Time step (seconds)	Max. horizontal resolution (km)	Min horizontal resolution (km)	Max. biharmonic viscosity ($m^4\ s^{-1}$)	Max. Laplacian diffusivity ($m^2\ s^{-1}$)
NA025	$(1/4)^\circ \times (1/4)^\circ \cos\varphi$	544×336	2400	27.6	11.0	-1.5×10^{11}	300
LAB12	$(1/12)^\circ \times (1/12)^\circ \cos\varphi$	304×334	600	6.0	4.0	-2.0×10^{9}	70

for longitude and latitude, and has 46 vertical levels. More details can be found in Zhu et al. (2010). The LAB12 model covers the whole Labrador Basin and part of the Irminger Basin (from 49.2°N to 64.2°N and 61.5°W to 36.2°W, as indicated by the black box in Fig. 2). The refinement factor is 3, which obtains a horizontal resolution of $(1/12)^\circ \times (1/12)^\circ \cos\varphi$ (φ is latitude), i.e., between 4 km and 6 km (see Table 1). Considering some experiments have demonstrated that the topography-triggered instability near the west coast of Greenland is important for the formation of Irminger rings (Eden and Böning, 2002; Bracco and Pedlosky, 2003; Katsman et al., 2004; Bracco et al., 2008; Chanut et al., 2008), the bathymetry for LAB12 was derived directly from the 2-min resolution ETOPO2 bathymetry data of the National Geophysical Data Center (U. S. Department of Commerce et al., 2006), instead of interpolating from the NA025 topography. The same as in the NA025 setting (Zhu et al., 2010), the vertical mixing was parameterized by the 1.5 turbulent closure model of Gaspar et al. (1990), adapted to OPA by Blanke and Delecluse (1993). A Laplacian lateral isopycnal diffusion was used for tracers, with a diffusion coefficient equal to 70 $m^2\ s^{-1}$ at 49.2°N and decreasing poleward proportionally to the grid size. A horizontal biharmonic viscosity was used for momentum, with viscosity equal to $2.0 \times 10^9\ m^4\ s^{-1}$ at 49.2°N and decreasing poleward as the cube of the grid size.

The LAB12 and NA025 models were coupled together by the AGRIF package in a "two-way" nesting scheme. In particular, the NA025 simulations supplied boundary conditions for the LAB12 model, and the corresponding LAB12 simulations were used to update NA025 simulations over their overlapping areas. In addition, to dissipate the turbulent structures smaller than the coarse grid (NA025), a thin sponge layer (seven grid points of the LAB12 model) with enhanced Laplacian viscosity ($150\ m^2\ s^{-1}$) and diffusivity ($300\ m^2\ s^{-1}$) was added to four boundaries of their overlapping areas. As shown by the NA025 and LAB12 combined snapshots—for instance, potential temperature (i.e., within the LAB12 domain the potential temperature data are from LAB12, and outside it the NA025 data are used; figures not shown here)—the contrast between two grids due to different grid space was clear. However, along their interfaces the temperature showed a high consistency; for example, at the northeastern corner of the interface, the inflow of the warm/salty Irminger water from the NA025 region into the LAB12 region was clear and continuous.

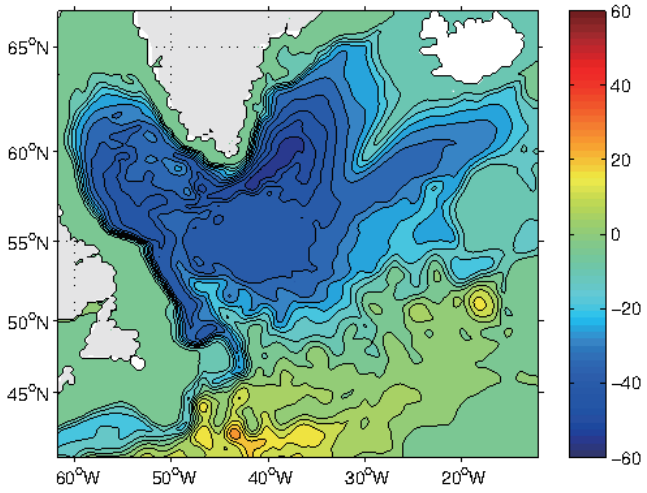

Fig. 2. Mean barotropic streamfunction (Sv) from NA025 in the subpolar North Atlantic Ocean. Contour interval is 5 Sv.

In our experiments, a so-called spectral nudging scheme (Thompson et al., 2006) was applied for model temperature and salinity in the upper three levels, to reduce the forcing uncertainties. The nudging coefficients corresponded to the time scale of 5 days, 10 days and 20 days for the 1st, 2nd and 3rd level, respectively. In addition, considering the existence of sea ice at high latitudes, no nudging was applied for temperature in the regions north of 50°N. Meanwhile, the spectral nudging was always applied for the layer between depths of 450 m and 1500 m in the Gulf of Cadiz, which was done in light of the fact that current OGCMs find it hard to represent the "overflow" process of Mediterranean water masses into the North Atlantic Ocean (Molines et al., 2007).

2.2. *Initialization and datasets*

Initial conditions for temperature and salinity were derived from the WOA05 (World Ocean Atlas 2005) dataset (Antonov et al., 2006; Locarnini et al., 2006) for the North Atlantic and Baltic Sea, and from the MEDAR (MEDiterranean Data Archaeology and Rescue) dataset (Brankart and Brasseur, 1998) for the Mediterranean Sea. The NA025 model was initialized from a 10-yr NA025 spin-up run forced with climatological monthly mean atmospheric fields [i.e., experiment EXP1 in Zhu et al. (2010), where all model levels were spectrally nudged]. The LAB12 model was initialized from the state after two years of the embedded system run, in which both NA025 and LAB12 were initialized at rest. The embedded system was then run for another 20 years, forced by the climatological monthly mean atmospheric fields from NCEP–NCAR (National Centers for Environmental Prediction–National Center for Atmospheric Research) reanalysis data (Kalnay et al., 1996).

In the following sections, all diagnostics (including mean states) are based on the last 5 years (from the 26th to 30th year) of model simulations, which was stored as averaged fields every five days. In presenting the results from the eddy-resolving simulation, when domains were larger than LAB12, outputs from NA12 were used; otherwise, outputs from LAB12 were used. In addition, to explore the impact of mesoscale eddies on the lateral positioning of deep convection, results from the eddy-resolving simulation were compared with another prognostic run; namely, experiment EXP3 in Zhu et al. (2010). The EXP3 configuration was the same as NA025 in terms of topography, forcing and initialization of the North Atlantic circulation, but with no LAB12 embedded, which meant it was eddy-permitting only. More details

about EXP3 can be found in Zhu et al. (2010).

3. Circulation characteristics in the Labrador Sea

Figure 2 shows the average barotropic streamfunction from NA025 in the Subpolar North Atlantic Ocean. The region was characterized by a cyclonic circulation with volume transport in the boundary current between 40 and 50 Sv, which consisted of 30–40 Sv "throughput" in the Subpolar grye and 10–15 Sv in the local recirculation, in good agreement with observational estimates (Pickart et al., 2002). The internal recirculation cells in the Labrador Sea (and the Irminger Sea) have been discovered by in situ studies (Lavender et al., 2000). In the simulations, cyclonic recirculations were clearly shown in the western Labrador basin and the western Irminger basin. A third recirculation, located southwest of Greenland and shown in Lavender et al. (2000), was not so discernable, and seemed to be combined with the one in the western Irminger basin. The favorable representation of the recirculation might have resulted from the more realistic representation of the bottom topography by partial cell (Käse et al., 2001; Zhu et al., 2010) than by full cell. The internal recirculations may play an important role for the dynamics of the two basins by influencing the spreading of the intermediate and deep water masses in the Labrador and Irminger Seas (Straneo et al., 2003).

Lazier and Wright (1993) identified the deep Labrador Current as a current with a significant barotropic component near the 2500 m isobath offshore of Labrador. The flow is reported to exhibit a clear seasonal variability in speed with a maximum in winter and a minimum in summer. Over the last two decades, the Labrador Current was monitored during seven cruises (Dengler et al., 2006) along two sections perpendicular to the shelf break in the Labrador Sea (see Fig. 1). These two sections locate at about 53°N (referred to as the 53°N section) and along the western part of WOCE (World Ocean Circulation Experiment) line AR7W at about 56°N (referred to as the 56°N section), respectively. Here, we present our model simulations along the same sections, and discuss the similarities/differences between simulations and observations.

Figure 3 shows the 5-yr mean alongshore component of the LAB12 model current in the 56°N (Fig. 3a) and 53°N (Fig. 3b) sections. The current resembled the major elements of the observed alongshore velocity component [see Fig. 3 in Dengler et al. (2006)], which in the two sections has a strong barotropic component with intense velocities at all levels from the surface down to the bottom. The simulated deep Labrador Current in the 56°N section was mostly confined within about 100 km offshore, and there was a weak southeastward flow from 100 km to 170 km offshore. It was slightly narrower than the observed extension ($\sim$ 120 km) during 1996–2005 (Dengler et al., 2006). Further offshore from the Labrador Current, a weak northwestward flow was present in the simulations, which was the counter-current recirculation as mentioned above (Lavender et al., 2000). Compared to the observations by Dengler et al. (2006), the simulated counter-current recirculation was narrower and weaker. A similar difference appeared in the 53°N section. The simulated deep Labrador Current in the 53°N section extended from the shelf break to about 120 km offshore, also slightly narrower than the 140 km estimated by Dengler et al. (2006) based on 1996–2003 mean observations. The simulated recirculation in this section was stronger than that in the 56°N section, but still weaker than observations (Dengler et al., 2006). In general, the model realistically represented the observed climatologic features of the Labrador Current in the two sections.

Figure 4 presents the seasonal anomalies of alongshore velocities from LAB12 in the 56°N and 53°N sections rela-

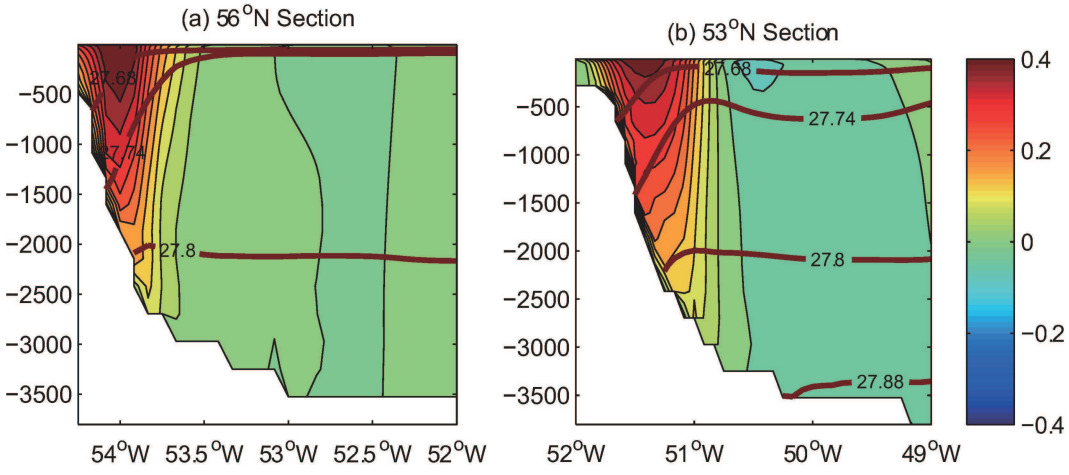

Fig. 3. Mean alongshore velocities from LAB12 for the (a) 56°N and (b) 53°N sections. Contour interval is 0.04 m s^{-1}. The contours in red are potential densities with reference to the surface. Positive (negative) represents southeastward (northwestward) flow. The vertical axis is depth in meter.

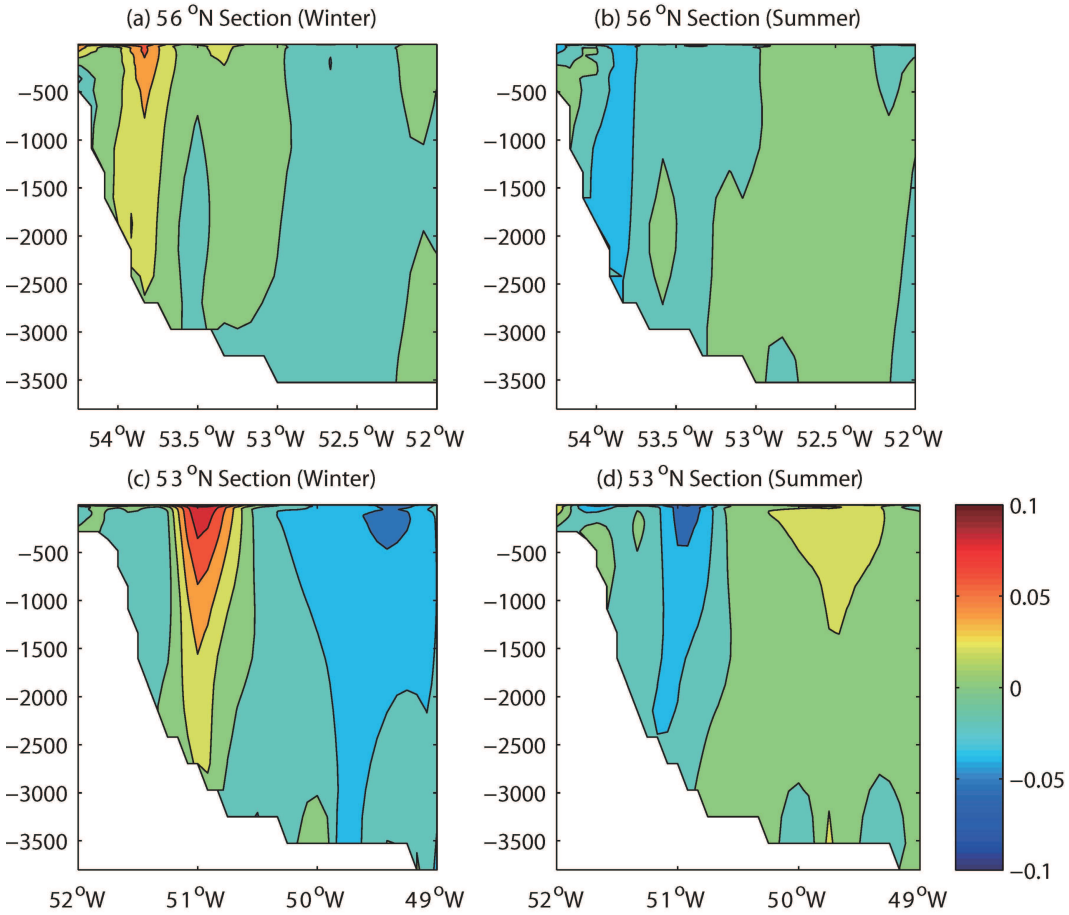

Fig. 4. Seasonal anomalies (relative to the annual mean, i.e., Fig. 3) of alongshore velocities from LAB12 for the (a) 56°N and (b) 53°N sections: (a, c) for winter (Jan–Mar); (b, d) for summer (Jul–Sep). Contour interval is 0.02 m s^{-1}. The vertical axis is depth in meter.

tive to their annual mean (i.e., Fig. 3). It can be seen that, in both sections, the deep Labrador Current was significantly stronger in winter than in summer, which was consistent with the observational estimates (Lazier and Wright, 1993). Offshore from the deep Labrador Current, the counter-current recirculation also exhibited similar seasonal variations, i.e., strong in winter and weak in summer. In addition, the simulated seasonal variations in the 53°N section were generally higher than in the 56°N section.

4. Mesoscale eddies in the Labrador Sea

In this section we discuss the mesoscale eddies simulated by the LAB12 model by exploring their characteristics and possible generation mechanisms. As in the previous section, we start by comparing the model results with some available observational studies.

4.1. *Distribution of surface eddy kinetic energy*

The model surface eddy kinetic energy (EKE) was defined as

$$\mathrm{EKE} = \frac{1}{2}\overline{(u'^2 + v'^2)}\,,$$

where primes were defined as the deviations of the surface horizontal velocities from their monthly average over the last five years of simulations. It should be noted that our model output storage strategy, i.e., 5-day average, might have underestimated the diagnosed eddy kinetic energy in contrast to instantaneous fields. Figure 5 shows the distribution of annual mean surface eddy kinetic energy in the Labrador Sea obtained from LAB12. The spatial pattern of simulated EKE in the Labrador Sea was similar to that derived from Topex-Poseidon satellite altimeter data (Lilly et al., 2003), while the magnitude of the simulated EKE in the areas of strong mesoscale variability was underestimated compared with observations. For instance, the localized EKE maximum near the west coast of Greenland was about 100–150 $cm^2\ s^{-2}$, which was smaller than the lower branch of the reported range of 200–500 $cm^2\ s^{-2}$ (White and Heywood, 1995; Ducet et al., 2000; Fratantoni, 2001; Stammer et al., 2001; Prater, 2002; Lilly et al., 2003). Particularly, in the model simulations (Fig. 5), there were generally two regions with enhanced mesoscale activities: one located near the west coast of Greenland, which was associated with the energetic Irminger rings; and the other in the northwest corner

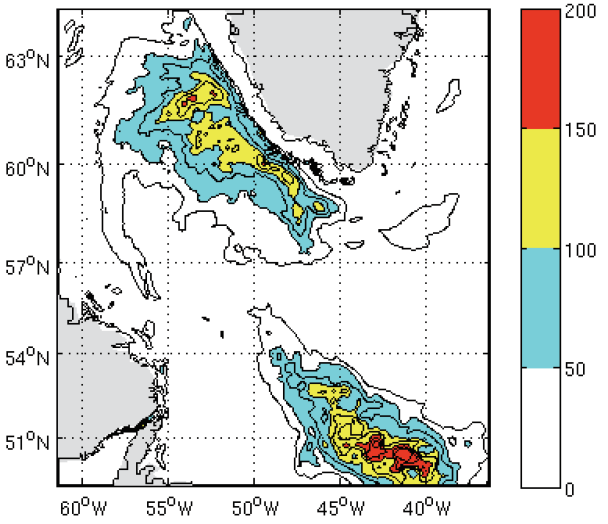

Fig. 5. Distribution of surface eddy kinetic energy ($cm^2\ s^{-2}$) over the Labrador Sea from LAB12.

of the North Atlantic Current (NAC). Moderate mesoscale variability was also shown along the rim of the convection patch. These mesoscale activities were associated with the steep isopycnal slopes after deep convection, which can result in baroclinic instability (see section 4.2). On the other hand, the boundary current eddies, such as along the Labrador Current, were not well represented in the current LAB12 simulations, as compared with satellite altimeter data (Lilly et al., 2003). In another experiment with the resolution increased from (1/12)° to (1/16)° (not shown here), the boundary current eddies were reasonably simulated, which implies that (1/12)° was still not high enough to resolve the boundary current eddies and may possibly be a major factor for underestimating general eddy activities in comparison with observations.

From the snapshots of potential temperature and relative vorticity in winter and summer (not shown here), it was found that in both seasons a number of Irminger rings with warm cores occurred along the west coast of Greenland, and most of them were anticyclonic. The simulations also showed there to be a greater abundance of Irminger rings in winter than in summer, which is consistent with the seasonal cycle of eddy kinetic energy in the Labrador Sea (Eden and Böning, 2002). In addition, another difference between winter and other seasons was also present in the snapshots: in winter, a convection patch formed in the southwest part of the Labrador Sea as a result of deep convection, and some mesoscale activities were clearly intensified along the rim of the patch, which were not seen in other seasons (e.g., summer).

4.2. *Baroclinic and barotropic energy transfers*

Among the three types of eddies in the Labrador Sea, Irminger rings are the most energetic, which form from Irminger Sea water in the eastern part of the Labrador Sea and can propagate to the central basin. The mechanism of their generation is discussed in a number of previous studies (Eden and Böning, 2002; Bracco and Pedlosky, 2003; Katsman et al., 2004; Bracco et al., 2008), but nevertheless remains a matter of debate. Eden and Böning (2002) suggested that the mechanism for the instability is mainly barotropic, based on an analysis of the energy conversion rates between 100-m and 400-m depths. In contrast, Bracco and Pedlosky (2003) and Bracco et al. (2008) used two slightly different idealized quasigeostrophic channel models, and suggested that the Irminger ring formation mechanism might be associated with local baroclinic instability induced by the variable topography. Katsman et al. (2004), using the Massachusetts Institute of Technology primitive equation model in an idealized configuration, concluded that the instability process is mixed, with barotropic energy conversion prevailing in the upper water column and baroclinic conversion dominating at intermediate depths.

In the present study, we revisited the problem by calculating the baroclinic (BC_{ET}) and barotropic (BT_{ET}) components of energy transfer between mean and eddy flows. The calculations were made as follows (Wright, 1981; Eden and Böning, 2002; Demirov and Pinardi, 2007):

$$BC_{ET} = -\rho_0 \left(\frac{g}{N\rho_0}\right)^2 \left(u'\rho' \frac{\partial \tilde{\rho}}{\partial x} + v'\rho' \frac{\partial \tilde{\rho}}{\partial y}\right),$$

and

$$BT_{ET} = -\rho_0 \left[u'u' \frac{\partial \tilde{u}}{\partial x} + u'v' \left(\frac{\partial \tilde{u}}{\partial y} \frac{\partial \tilde{v}}{\partial x}\right) + v'v' \frac{\partial \tilde{v}}{\partial y}\right],$$

where ρ is the *in situ* density, and $\rho_0, \tilde{\rho}(x,y,z,t), \rho'(x,y,z,t)$ represent the density scale (1020 kg m^{-3}), the seasonal cycle, and the perturbation density, respectively; N is Brunt–Väisälä frequency ($N^2 = -g\rho_0^{-1}\partial\sigma/\partial z$; σ is the potential density), and its time- and space-mean values were applied in the calculations (note that the horizontal mean was based on the whole North Atlantic Ocean, but with the Hudson Bay, the Baltic Sea and the Mediterranean Sea excluded); $\tilde{u}(x,y,z,t), \tilde{y}(x,y,z,t)$ are the east and north components of the (monthly) seasonal cycle component of the velocity field; and $u'(x,y,z,t), y'(x,y,z,t)$ are eddy components of the velocity fields. Positive (negative) BC_{ET} and BT_{ET} values indicate an energy transfer from (to) the mean flow to (from) the eddy fields.

Figure 6 shows the mean baroclinic (Figs. 6a and c) and barotropic (Figs. 6b and d) energy transfer rates obtained by vertically integrating for the uppers layers from 16 m to 418 m deep (Figs. 6a and b) and the intermediate layers from 418 m to 2008 m deep (Figs. 6c and d). Note that in order to use the same color bar with Fig. 6b, the value in Fig. 6a was multiplied by a factor of 5. The distribution of the baroclinic transfer rate (Figs. 6a and c) on the shelf and shelf slope, with extremely large negative and positive values often seen in close areas, was patchy and might be unrealistic, possibly associated with the fact that the boundary current eddies were not well represented by the current resolution. Roughly speaking, except in the shelf region, both baroclinic and barotropic transfers exhibited similar patterns in the surface and intermediate layers. Over the two layers, the barotropic transfer

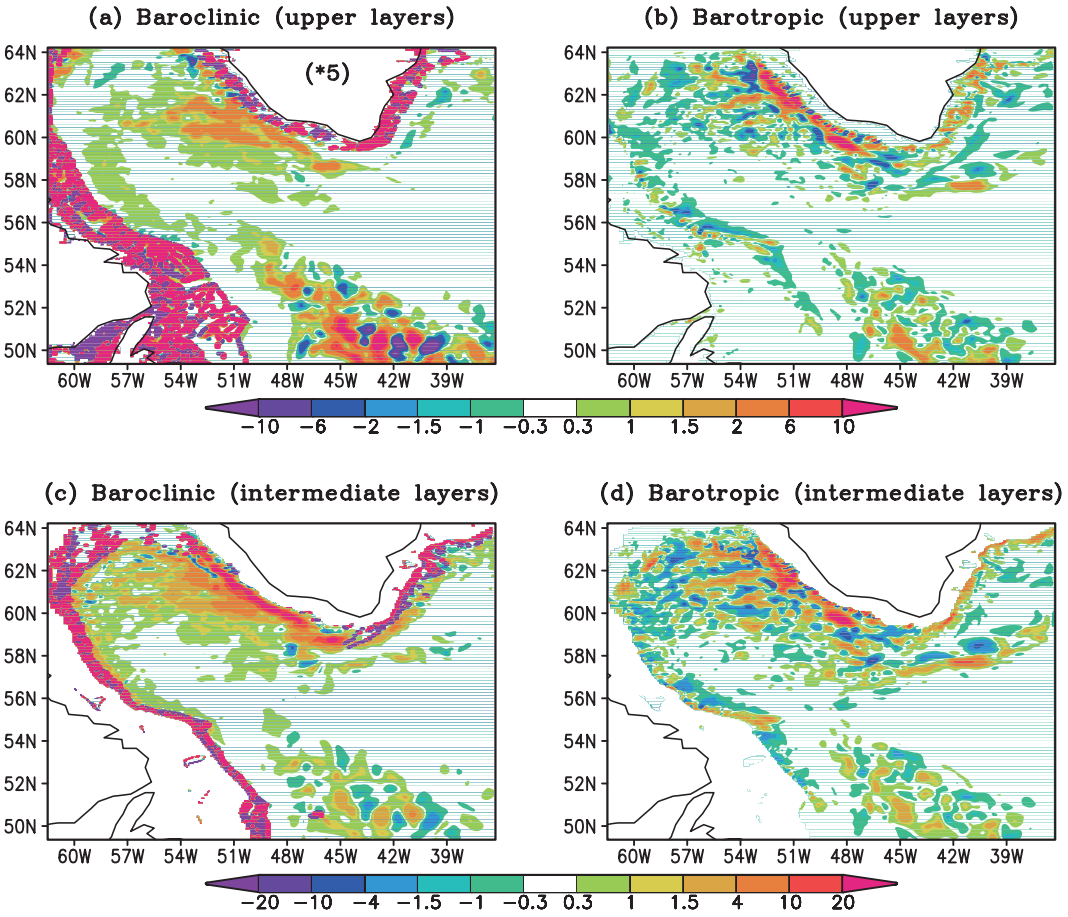

Fig. 6. The depth-integrated (a, c) baroclinic energy transfer rate and (b, d) barotropic energy transfer rate (in 10^{-3} J m^{-2} s^{-1}), based on the LAB12 output: (a, b) for the upper layers from 16 m to 418 m; (c, d) for the intermediate layers from 418 m to 2008 m. Panels (a, b) and (c, d) share the same colored bars, respectively. Absolute values of energy flux $< 0.3 \times 10^{-3}$ J m^{-2} s^{-1} are not shown. Note that to use the same colored bar as in (b), the values in (a) are multiplied by a factor of 5.

had a close order of magnitude, but the baroclinic transfer rate was clearly stronger over the surface layer than the intermediate layer. Generally, the baroclinic transfer was significantly lower than the barotropic transfer over the surface layer, but they were equivalent over the intermediate layer where the Irminger Water stayed.

In addition, it was also found that the baroclinic and barotropic transfers made different contributions to the local mesoscale variability. Over the formation area of active Irminger rings, i.e., off the west coast of Greenland, positive values of the baroclinic and barotropic transfer rates indicated that both processes were consistently making contributions to the eddy formation, with the barotropic process contributing more in the surface layer and both equivalently in the intermediate layer. Slightly away from the formation region to the interior basin, both positive and negative values coexisted in the barotropic transfers, while coherent positive values appeared in the baroclinic transfers. This implies that, when the energetic Irminger rings were propagating to the interior basin, the baroclinic process was still favoring their formation and thus sustained their long lifetime. On the other hand, when the barotropic process played the same role as the baroclinic process in energizing Irminger rings, it also dispersed the eddies by converting the eddy energies to mean flow, collapsing the Irminger rings and shortening their lifetime. Therefore, our analysis indicates that baroclinic and barotropic processes play different roles in the life cycle of Irminger rings. Particularly, while their generation is attributed to a mixed process of both baroclinic and barotropic instabilities, they will be collapsed by the barotropic process when propagating to the interior basin.

In addition, along the rim of the convection patch in the interior Labrador Sea, there was also a coherent moderate positive baroclinic transfer (Figs. 6a and c). This baroclinic instability was due to the steep isopycnal slopes after deep convection, which would have contributed to the formation of the convective eddies in the Labrador Sea.

5. Deep convection in the Labrador Sea: the effects of mesoscale eddies

In this section we explore the effects of mesoscale eddies on the positioning of deep convections in the Labrador Sea

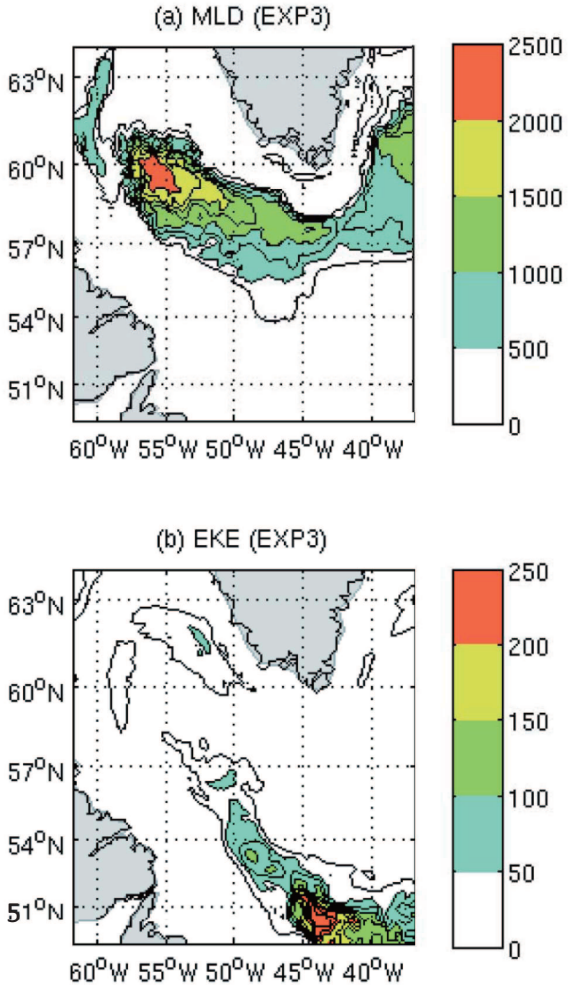

Fig. 7. (a) Five-year mean mixed layer depths (units: m) in the Labrador Sea at the end of March from EXP3. (b) Distribution of surface eddy kinetic energy ($cm^2\ s^{-2}$) over the Labrador Sea from EXP3.

by comparing simulations from the above eddy-resolving simulation and an eddy-permitting run (EXP3 in Zhu et al., 2010). Figure 7a shows the simulated mixed layer depth from EXP3 simulations (the mixed layer depth is defined as the depth where potential density exceeds the surface density by 0.01 kg m^3). The model results did not suffer from the "excessive convection" problem as found in other models with similar or lower resolutions (Willebrand et al., 2001; Tréguier et al., 2005), but some biases were still evident in comparison with observations (Lavender et al., 2000; Pickart et al., 2002). In particular, the position of the highest mixed layer depth was clearly unrealistic, with biases toward the northeastern basin. When the results were plotted along the AR7W section (not shown here), the mixed layer depth clearly shifted toward the Greenland side in contrast to reality where it slopes to the Labrador side (Lavender et al., 2000; Pickart et al., 2002).

This bias in the eddy-permitting model was largely related to the improper representation of the position of the isopycnal dome in the Labrador Sea. In hydrographic data (Pickart et al., 2002; Igor Yashayaev, 2009, personal communication), the climatological potential temperature isolines clearly dome toward the Labrador side along the AR7W section, which implies that the low stratification area is located close to the Labrador side. Under the oceanic condition, deep convection will be evoked on the Labrador side when substantial oceanic heat loss happens in winter. However, the hydrographic conditions in the eddy-permitting model were opposite to reality, where the simulated mean potential temperature and potential density isolines clearly sloped toward the Greenland side along the AR7W section (Fig. 8a), and consequently deep convection was unrealistically evoked on the Greenland side in winter. On the other hand, due to its relatively low resolution, the eddy-permitting model only represented limited mesoscale activities in the Labrador Sea. As shown in Fig. 7b, there were low EKEs in the whole basin except for the northwest corner of the NAC. We suggest that the unrealistic deep convection lateral position might have been related to a lack of mesoscale activities in EXP3. When the mesoscale activities (especially Irminger rings) in the Labrador Sea are well represented as in LAB12, deep convection will be evoked in a realistic position.

5.1. *Deep convection in the eddy-resolving simulations*

Deep convection was significantly improved in the LAB12 simulations regarding the location of intense vertical mixing. Figure 9a shows the mean mixed layer depths in March, with the mean surface velocity superimposed in vectors. At the surface, the West Greenland Current (WGC), East Greenland Current (EGC) and Labrador Current (LC) constituted an important part of the cyclonic circulation in the subpolar North Atlantic. Within the cyclonic circulation, the most active deep convection happened on the Labrador side, in which the maximum mixed layer depths were more than 2200 m. Figure 9b shows a snapshot of mixed layer depth, with eddy component velocity overlaid in vectors. There were two regions with a high level of mesoscale activities—along the NAC and along the west coast of Greenland, corresponding to two active mesoscale activity regions in the EKE map (Fig. 5). From Fig. 9b, it is confirmed that eddies along the west coast of Greenland (i.e., Irminger rings) clearly affected the sites of deep convection, which were farther south-southwest and more realistic in comparison with the above eddy-permitting simulations. Figure 9c shows the time series of potential temperature at the deep convection site [averaged within 100 km of (57.5°N, 54°W)]. The seasonal cycle of the temperature at the site of deep convection was realistically simulated by the eddy-resolving model. At the end of winter when deep convection was well developed, a cold patch extended vertically to more than 1500 m deep. From April, the subsurface re-stratification began to build up, and was fully established in the following January. Generally, the characteristics of the simulated deep convection were in good agreement with wintertime surveys by Clarke and Gascard (1983) and Pickart et al. (2002).

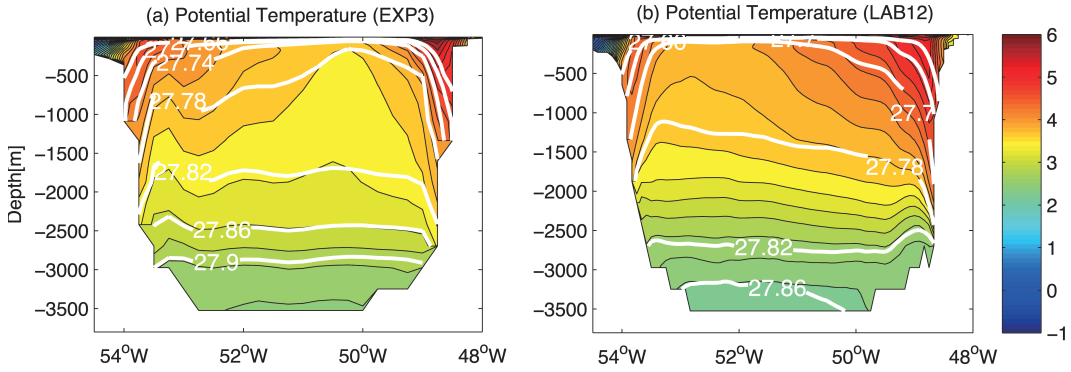

Fig. 8. Climatological mean potential temperature (°C; colors) and potential density (with reference to the surface; units: kg m^{-3}, in contours) along the WOCE AR7W section from (a) EXP3 and (b) LAB12.

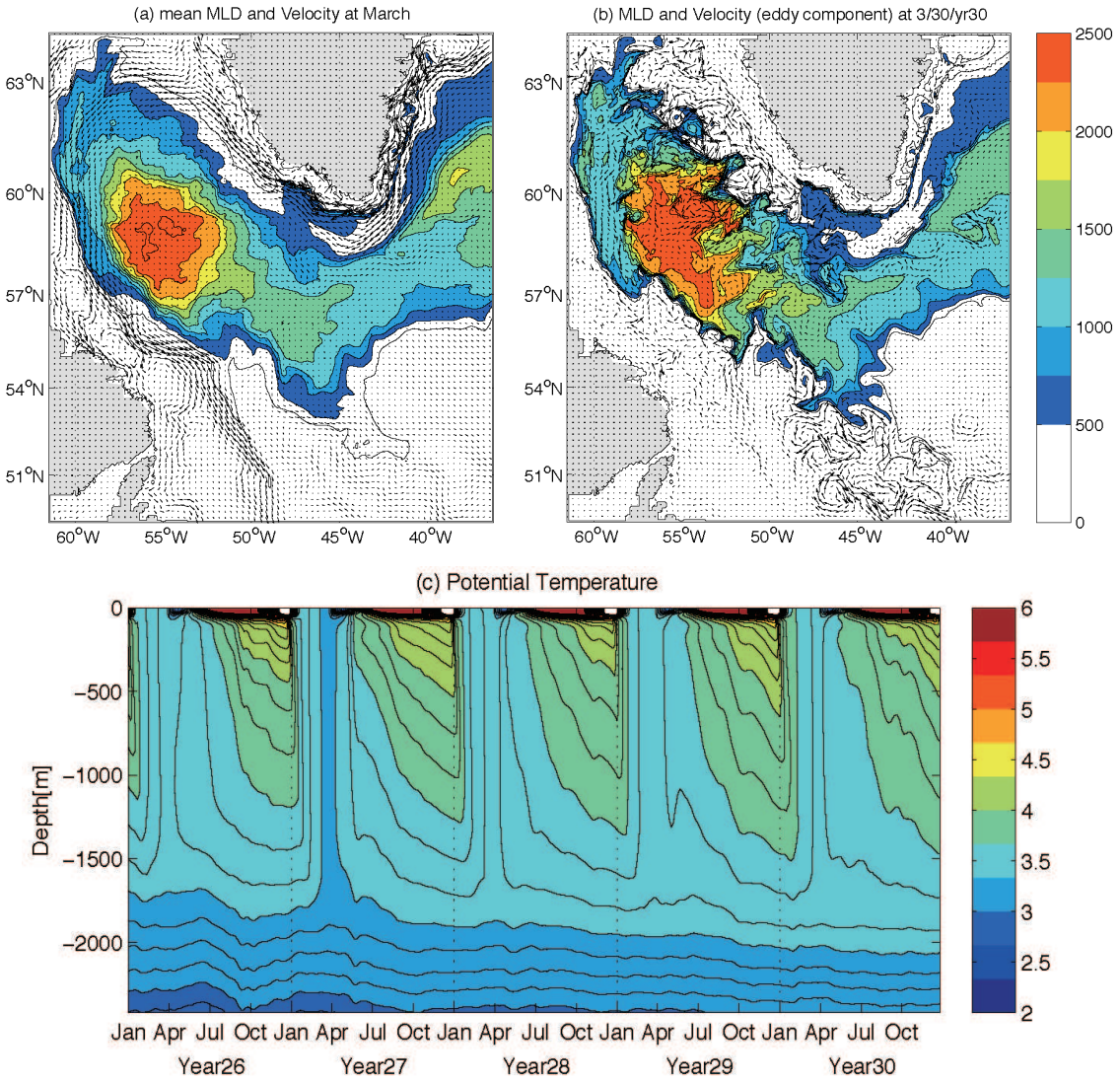

Fig. 9. (a) Mean mixed layer depth (units: m) in March, with mean surface velocity overlaid in vectors. (b) A snapshot of mixed layer depth (units: m) at the end of March 0030, with eddy component velocity [relative to mean velocity in (a)] overlaid. (c) Time evolution of the vertical temperature profile (units: °C) at the observed deep convection site by Pickart et al. (2002) [averaged within 100 km of (57.5°N, 54°W)]. The velocity fields in (a, b) have been sub-sampled every four grid points for clarity of presentation.

5.2. *Lateral eddy heat flux*

From the comparison of deep convection positions in the models with and without Irminger rings resolved, it can be concluded that the presence of Irminger rings have an important effect on positioning deep convection in the Labrador Sea. To explore the possible cause, the lateral eddy heat flux was calculated based on the eddy-resolving model (LAB12) simulations. Figure 10 presents the vertically-averaged eddy heat flux ($\overline{u'T'}, \overline{v'T'}$) over the middle-upper layers from 170 m to 1210 m, with the mean temperature superimposed as contours. As shown in the above section, deep convection in the LAB12 simulations could develop to a depth of 2000 m in the Labrador Sea in winter, and the stability of the middle-upper water columns was important for the development of deep convection. Figure 10 indicates that, in the Labrador Sea, the most intense lateral eddy heat flux was present off the west coast of Greenland, where the most energetic eddies (i.e., Irminger rings) formed and moved toward the interior basin. Through the lateral eddy flux, lots of heat was transported from the warm boundary currents to the interior Labrador Sea. Thereby, the water columns in the eastern basin were stratified and stabilized. The stabilization over the west coast of Greenland was clearly shown in the mean potential temperature along the AR7W section in the eddy-resolving model simulations (Fig. 8b). Along the section, the simulated potential temperature isoline sloped toward the Labrador side, which is consistent with the hydrographic data (Pickart et al., 2002; Rykova et al., 2009; Igor Yashayaev, 2009, personal communication). Under the oceanic conditions, it was difficult for deep convection to develop over the west coast of Greenland. Therefore, the lateral eddy flux related to Irminger rings confined deep convection within a small region in the southwest part of the Labrador Sea. In the eddy-permitting models, Irminger rings and the associated lateral eddy fluxes cannot be represented; consequently, deep convection would strongly follow the surface heat flux loss and happen in an unrealistic area.

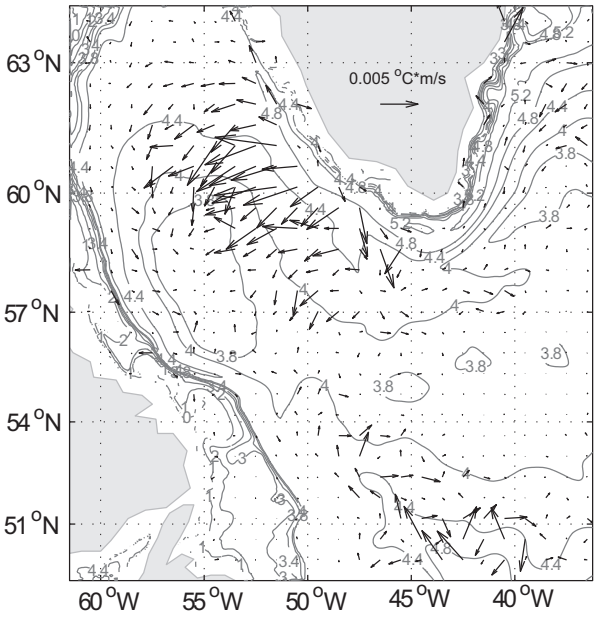

Fig. 10. Vertically-averaged (between 170 and 1210 m) eddy heat flux (vectors, units: °C × m s^{-1}) and mean temperature (contours, units: °C) based on the LAB12 output.

6. Discussion and conclusion

In this paper, simulations from an eddy-resolving ocean model have been presented for the Labrador Sea, including the general circulation characteristics, mesoscale eddies, and its deep convection. The results showed the internal recirculations and the annual variation of the deep Labrador Current to be well represented. As for the mesoscale eddies, the distribution of the surface eddy kinetic energy was close to that derived from Topex-Poseidon satellite altimeter data, but its amplitude was underestimated. The boundary current eddies were also not well resolved in the current (1/12)° configuration. The eddy-mean flow energy transfer was further diagnosed. The results suggested that, over the region off the west coast of Greenland, both baroclinic and barotropic processes make contributions to the generation of Irminger rings; but when they propagate to the interior basin, the baroclinic process still favors their formation and sustains them for longer. However, the barotropic process starts to disperses their energy of the eddies. In addition, along the rim of the convection patch in the interior Labrador Sea in winter, the baroclinic process generates moderate convective eddies. Meanwhile, in contrast with previous eddy-permitting simulations, deep convections in the Labrador Sea was well represented regarding their lateral position, which was realistically confined within a region in the southwest part of the Labrador basin. Further analysis indicated that the lateral eddy flux associated with Irminger rings could explain the improvement. The lateral eddy flux contributes to a realistic position of the isopycnal dome in the Labrador Sea, which makes deep convection happen at a realistic site.

Our results may raise a question for the broader climate community. In the current Intergovernmental Panel on Climate Change (IPCC) assessment (Solomon et al., 2007), and also the impending next assessment, it is reported that few coupled systems can afford an eddy-resolving ocean model. Considering the vital role of the Labrador Sea (and the associated LSW coming from deep convection events) in the global climate, the eddy effects have to be realistically parameterized. However, in existing parameterization schemes such as the Gent–McWilliams scheme (Gent and McWilliams, 1990), only the baroclinic instability process is taken into account. Therefore, it will be interesting to see an estimation of the climate change uncertainties in the current IPCC assessment that are associated with the lack of the proper eddy processes. On the other hand, considering the mixed essence of Irminger rings, more advanced schemes should be developed for the Labrador Sea, which should include both the baroclinic and barotropic processes.

Acknowledgements. This work was funded by the Canadian Foundation for Climate and Atmospheric Science through projects GOAPP and GR-631 and NSERC. The support of ACEnet (the Atlantic Computational Excellence Network), which provided the computing assistance for this work, is greatly acknowledged. We also thank Laurent Debreu for her help in applying the AGRIF package.

REFERENCES

Antonov, J. I., R. A. Locarnini, T. P. Boyer, A. V. Mishonov, and H. E. Garcia, 2006: *World Ocean Atlas 2005*, *Volume 2: Salinity*. S. Levitus, Ed. NOAA Atlas NESDIS 62, U. S. Government Printing Office, Washington, D. C., 182 pp.

Blanke, B., and P. Delecluse, 1993: Low frequency variability of the tropical Atlantic Ocean simulated by a general circulation model with mixed layer physics. *J. Phys. Oceanogr.*, **23**, 1363–1388.

Blayo, E., and L. Debreu, 1999: Adaptive mesh refinement for finite-difference ocean models: First experiments. *J. Phys. Oceanogr.*, **29**, 1239–1250.

Bracco, A., and J. Pedlosky, 2003: Vortex generation by topography in locally unstable baroclinic flow. *J. Phys. Oceanogr.*, **33**, 207–219.

Bracco, A., J. Pedlosky, and R. Pickart, 2008: Eddy formation near the West coast of Greenland. *J. Phys. Oceanogr.*, **38**, 1992–2002.

Brankart, J.-M., and P. Brasseur, 1998: The general circulation in the Mediterranean Sea: A climatological approach. *J. Mar. Syst.*, **18**, 41–70.

Chanut, J., B. Barnier, W. Large, L. Debreu, T. Penduff, J. M. Molines and P. Mathiot, 2008: Mesoscale eddies in the Labrador Sea and their contribution to convection and restratification *J. Phys. Oceanogr.*, **38**, 1617–1643.

Clarke, R. A., and J.-C. Gascard, 1983: The formation of Labrador Sea Water. Part I: Large-scale processes. *J. Phys. Oceanogr.*, **13**, 1764–1778.

Cooke, M. A., E. Demirov, and J. Zhu, 2014: A model study of the relationship between sea-ice variability and surface and intermediate water mass properties in the Labrador Sea. *Atmosphere-Ocean*, **52**(2), 142–154, doi: 10.1080/07055900.2013.877417.

Debreu, L., E. Blayo, and B. Barnier, 2005: A general adaptive multi-resolution approach to ocean modelling: Experiments in a primitive equation model of the North Atlantic. *Adaptive Mesh Refinement: Theory and Applications*. Vol. 41, *Lecture Notes in Computational Science and Engineering*, T. Plewa et al., Eds., Springer, 303–314.

Demirov, E. K., and N. Pinardi, 2007: On the relationship between the water mass pathways and eddy variability in the western Mediterranean Sea. *J. Geophys. Res.*, **112**, C02024, doi: 10.1029/2005JC003174.

Dengler, M., J. Fischer, F. A. Schott, and R. Zantopp, 2006: Deep Labrador Current and its variability in 1996–2005. *Geophys. Res. Lett.*, **33**, L21S06, doi: 10.1029/2006GL026702.

Ducet, N., P. Y. Le Traon, and G. Reverdin, 2000: Global high-resolution mapping of ocean circulation from TOPEX/ Poseidon and ERS-1 and -2. *J. Geophys. Res.*, **105**(C8), 19 477–19 498.

Eden, C., and C. Böning, 2002: Sources of eddy kinetic energy in the Labrador Sea. *J. Phys. Oceanogr.*, **32**, 3346–3363.

Fichefet, T., and M. A. M. Maqueda, 1997: Sensitivity of a global sea ice model to the treatment of ice thermodynamics and dynamics. *J. Geophys. Res.*, **102**, 12 609–12 646.

Fratantoni, D. M., 2001: North Atlantic surface circulation during the 1990's observed with satellite-tracked drifters. *J. Geophys. Res.*, **106**, 22 067–22 093.

Gao, Y. Q., and L. Yu, 2008: Subpolar gyre index and the North Atlantic meridional overturning circulation in a coupled climate model. *Atmospheric and Oceanic Science Letters*, **1**, 29–32.

Gaspar, P., Y. Grégoris, and J.-M. Lefevre, 1990: A simple eddy kinetic energy model for simulations of the oceanic vertical mixing Tests at station papa and long-term upper ocean study site. *J. Geophys. Res.*, **95**, 16 179–16 193.

Gent, P. R., and J. C. McWilliams, 1990: Isopycnal mixing in ocean circulation models. *J. Phys. Oceanogr.*, **20**, 150–155.

Hátún, H., C. C. Eriksen, and P. B. Rhines, 2007: Buoyant eddies entering the Labrador Sea observed with gliders and altimetry. *J. Phys. Oceanogr.*, **37**, 2838–2854.

Kalnay, E., and Coauthors, 1996: The NCEP/NCAR 40-Year Reanalysis Project. *Bull. Amer. Meteor. Soc.*, **77**, 437–472.

Käse, R. H., A. Biastoch, and D. B. Stammer, 2001: On the mid-depth circulation in the Labrador and Irminger seas. *Geophys. Res. Lett.*, **28**, 3433–3436.

Katsman, C. A., M. A. Spall, and R. S. Pickart, 2004: Boundary current eddies and their role in the restratification of the Labrador Sea. *J. Phys. Oceanogr.*, **34**, 1967–1983.

Lavender, K. L., R. E. Davis, and W. B. Owens, 2000: Mid-depth recirculation observed in the interior Labrador and Irminger seas by direct velocity measurements. *Nature*, **407**, 66–69.

Lazier, J. R. N., and D. G. Wright, 1993: Annual velocity variations in the Labrador Current. *J. Phys. Oceanogr.*, **23**, 659–678.

Lilly, J. M., P. B. Rhines, F. Schott, K. Lavender, J. Lazier, U. Send, and E. D'Asaro, 2003: Observations of the Labrador Sea eddy field. *Progress in Oceanography*, **59**, 75–176.

Locarnini, R. A., A. V. Mishonov, J. I. Antonov, T. P. Boyer, and H. E. Garcia, 2006: *Temperature.* Vol. 1, *World Ocean Atlas* 2005, S. Levitus, Ed., NOAA Atlas NESDIS 61, U. S. Government Printing Office, Washington, D. C., 182 pp.

Madec, G., 2008: "NEMO reference manual, ocean dynamics component: NEMO-OPA. Preliminary version". Note du Pole de modélisation, Institut Pierre-Simon Laplace (IPSL), France, No 27.

Marshall, J., and F. Schott, 1999: Open-ocean convection: Observations, theory, and models. *Rev. Geophys.*, **37**, 1–64.

Molines, J. M., B. Barnier, T. Penduff, L. Brodeau, A., Treguier, S. Theetten, and G. Madec, 2007: Definition of the interannual experiment ORCA025-G70, 1958-2004. LEGI Report, LEGI-DRA-2-11-2006, 34 pp.

Pickart, R. S., D. J. Torres, and R. A. Clarke, 2002: Hydrography of the Labrador Sea during active convection. *J. Phys. Oceanogr.*, **32**, 428–457.

Prater, M. D., 2002: Eddies in the Labrador Sea as observed by profiling RAFOS floats and remote sensing. *J. Phys. Oceanogr.*, **32**, 411–427.

Rykova, T., F. Straneo, J. M. Lilly, and I. Yashayaev, 2009: Irminger current anticyclones in the Labrador Sea observed in the hydrographic record, 1990–2004. *J. Mar. Res.*, **67**, 361–384.

Solomon, S., and Coauthors, 2007: *Climate Change 2007: The Physical Science Basis*. Cambridge University Press, 996 pp.

Stammer, D., C. Böning, and C. Dieterich, 2001: The role of vari-

able wind forcing in generating eddy energy in the North Atlantic. *Progress in Oceanography*, **48**, 289–312.

Straneo, F., 2006: Heat and freshwater transport through the central Labrador Sea. *J. Phys. Oceanogr.*, **36**, 606–628.

Straneo, F., R. S. Pickart, and K. Lavender, 2003: Spreading of Labrador Sea Water: An advective-diffusive study based on Lagrangian data. *Deep-Sea Res. I*, **50**, 701–719.

Thompson, K. R., D. G. Wright, Y. Lu, and E. Demirov, 2006: A simple method for reducing seasonal bias and drift in eddy resolving ocean models. *Ocean Modelling*, **13**, 109–125.

Tréguier, A.-M., S. Theetten, E. Chassignet, T. Penduff, R. Smith, L. Talley, J. O. Beismann, and C. Böning, 2005: The North Atlantic subpolar gyre in four high-resolution models. *J. Phys. Oceanogr.*, **35**, 757–774.

U. S. Department of Commerce, National Oceanic and Atmospheric Administration, National Geophysical Data Center, 2006: 2-minute Gridded Global Relief Data (ETOPO2v2). [Available online at http://www.ngdc.noaa.gov/mgg/fliers/01mgg04.html].

White, M., and K. Heywood, 1995: Seasonal and interannual changes in the North Atlantic subpolar gyre from Geosat and TOPEX/POSEIDON altimetry. *J. Geophys. Res.*, **100**(C12), 24 931–24 941.

Willebrand, J., and Coauthors, 2001: Circulation characteristics in three eddy-permitting models of the North Atlantic. *Progress in Oceanography*, **48**, 123–161.

Wright, D. G., 1981: Baroclinic instability in Drake Passage. *J. Phys. Oceanogr.*, **11**, 231–246.

Zhu, J. S., E. Demirov, F. Dupont, and D. Wright, 2010: Eddy-permitting simulations of the Sub-polar North Atlantic: Impact of the model bias on water mass properties and circulation. *Ocean Dyn.*, **60**, 1177–1192, doi: 10.1007/s10236–010-0320–4.

Zhu, J., and E. Demirov, 2011: On the mechanism of interannual variability of the Irminger Water in the Labrador Sea. *J. Geophys. Res.*, **116**, C03014, doi:10.1029/2009JC005677.